Statistical Estimation of Daily Maximum and Minimum Air Temperatures from MODIS LST Data over the State of Mississippi

Georgy V. Mostovoy[1] and Roger L. King
GeoResources Institute, ERC, Mississippi State University, Mississippi State, Mississippi 39762

K. Raja Reddy and V. Gopal Kakani
Department of Plant and Soil Sciences, Mississippi State University, Mississippi State, Mississippi 39762

Marina G. Filippova
Department of Meteorology and Climatology, Moscow State University, 119992 Moscow, Russia

Abstract: Recent studies have shown that the Land Surface Temperature (LST) data measured by Moderate Resolution Imaging Spectro-Radiometer (MODIS) from both the Terra and Aqua platforms can be successfully used for linear regression estimates of daily maximum and minimum air temperatures at a local scale. Incorporation of these estimates into spatial interpolation schemes results in accuracy improvement of the surface air temperature, provided that the correlation coefficient (R) between the air temperature and LST is rather high. The purpose of this work was to examine the importance of pixel resolution (1.0 and 5.0 km²), satellite overpass time, season, land cover type, and the vegetation fraction (depending on the view zenith angle of the MODIS instrument) in controlling the observed level of R. The relative contribution of these factors in producing R variations has been assessed over the state of Mississippi during 2000–2004. Similarly, the sensitivity analysis of the difference between daily maximum and minimum air temperatures and LST to the same factors was performed. Results from these analyses have shown that R and the average difference between temperatures exhibited rather consistent variations depending on the above factors. The difference between maximum air temperature and LST increased linearly with the view angle (having typical range of 1–2°C for angle changes from 0° to ±65°) and remained constant or slightly decreased for daily air minimum temperatures. Both Terra and Aqua 1.0 km² LST exhibited a small but persistent increase of R between the air temperature and LST as compared with that of using 5.0 km² LST. Changing from Terra to Aqua LST did not alter significantly estimated values of R. This result suggested that the time difference between the moment of the satellite overpass and the time when maximum or minimum air temperature was observed was not critical for controlling the R value between the air temperature and LST at the involved spatial scales.

[1]email: mostovoi@gri.msstate.edu

INTRODUCTION

The air temperature (T_a) of the surface atmospheric boundary layer (ABL) represents an important element of a regional climate (Oke, 1987; Garratt, 1992). Therefore, daily maximum and minimum values of T_a are commonly used as an input in various environmental applications, including agricultural/forestry (Reddy et al., 1997; Régnière, 1996) and ecological models (Focks et al., 1995) to predict likely changes at field- and landscape-level attributes. The overall and differential spatial performance of these models is essentially dependent on the spatial/local accuracy of T_a fields (Reddy et al., 2002). Because routine meteorological observations (NOAA NCDC, 2004) are available at discrete points in space, typically separated by a distance of 30–50 km or more, a spatial interpolation is necessary to produce T_a data with a resolution ≤1.0 km^2.

Different interpolation schemes ranging from rather simple distance-weighted procedures to advanced methods utilizing knowledge about the observed spatial statistical structure of interpolated fields (Cressie, 1991), known as kriging interpolators, have been suggested and used for T_a estimates between observation points. Regional regression and kriging schemes (Bolstad et al., 1998; Florio et al., 2004) have been proven to be the most usable interpolators for daily or monthly averaged T_a fields.

The interpolation accuracy of both methods can be improved by the incorporation of any additional covariates related to T_a. Previous studies (Florio et al., 2004) demonstrated that use of Land Surface Temperature (LST) measured from a satellite as an additional covariate resulted in an improvement of T_a spatial estimates quality over the areas not covered with meteorological observations. The overall accuracy of temperature spatial interpolation using regional regression and kriging methods is about the same, with a typical value around 2°C. However, rather limited experiences of using LST in regression and kriging interpolation schemes, based mainly on Landsat and Advanced Very High Resolution Radiometer thermal infrared bands measurements, have been reported in literature. Unlike these satellite data, measurements from Moderate-Resolution Imaging Spectro-Radiometer (MODIS; MODIS, 2001) provide more comprehensive sets of LST products available from two platforms (Terra and Aqua), both with different spatial resolution (1.0 and 5.0 km^2). An approach has recently been suggested for spatial interpolation of T_a and T_s fields that involves a special fitting procedure of thin-plate smoothing spline to represent spatially distributed data available over a limited number of observation points (Prince et al., 2000). This method is of particular importance for the interpolation of noisy fields.

Remotely sensed LST has been amply used for field- and regional-scale estimates of the surface heat flux (Norman et al., 1995; Kustas et al., 1999), and much experience has been gained in this area. A rather close empirical relationship has been found between the local vegetation fractions described by the normalized vegetation index (NDVI) and surface skin temperature (Prihodko and Goward, 1997). Based on this finding, a method was developed to estimate T_a using remotely sensed LST and vegetation indices (Prince et al., 1998). This approach is known as the thermal-vegetation index (TVX) procedure, providing an estimate of a root mean square error in the range of 3–4°C for T_a. Much progress has also been achieved in integrating LST data into surface soil-vegetation/plant-ABL transfer (SVAT) models, resulting in

the accuracy improvement of spatial representation for basic environmental variables (Houborg and Soegaard, 2004). Generally, not only LST, but also other remotely sensed surface and atmospheric parameters (including biophysical characteristics of vegetation and their combinations) are assimilated into SVAT models. An example of improving yield prediction mapping by using leaf area index (LAI) estimates from MODIS surface spectral reflectance measurements and by assimilating these estimates into a crop simulation model has been reported by Doraiswamy et al. (2004).

The main objective of this study was to investigate point correlations between daily maximum/minimum air temperatures (available from operational measurements at the surface network of meteorological stations) and various MODIS LST products having different spatial resolutions and overpass times. It is important to evaluate seasonal and spatial variations of these correlations because they represent a necessary empirical basis for statistical interpolation methods including regional regression and kriging models, which use LST data to predict T_a. These methods cannot be applied successfully if correlations are low. A statistically based approach has been adopted in this study because it is quite difficult to properly consider different factors affecting LST remote sensing estimates and formulate a reliable physical model for accurate prediction of daily max/min T_a from LST data. A summary of these interacting factors, which control LST value, has been readily illustrated by Sandholt et al. (2002). Clear benefits of using remotely sensed LST for statistical estimating of daily max/min air temperatures have been documented in previous similar studies (Kawashima et al., 2000; Jones et al., 2004; Park et al., 2005). Jones et al. (2004) showed that statistical forecasting of daily minima from MODIS LST (late evening and night overpasses) could result in a better accuracy of predicted values and give more spatial details in comparison with National Weather Service operational forecasts and diagnostic fields based on surface observations. Statistical relationships between LST and the daily maximum of T_a and association of their difference with water budget factors have been reported recently by Park et al. (2005). The above studies are not numerous, covering only limited periods ranging from several days to a season. Therefore, a more comprehensive comparison in terms of extended temporal coverage (several years) and use of LST products from various satellite platforms with different spatial resolution (1.0 and 5.0 km^2)^2 is certainly relevant. It can be expected that the results of this comparison may facilitate a user's choice of the appropriate satellite platform and resolution among various LST MODIS products.

It should be clear that remotely sensed LST with a thermal infra-red (TIR) sensor is essentially the directional surface radiometric (temperature) or surface skin temperature (Norman and Becker, 1995; Jin et al., 1997). Note that symbols T_s and LST will be applied equally for this temperature throughout the paper. The adjective "directional," indicating angle dependence of surface emissivity, is generally omitted from the LST definition. LST spatial distribution depends critically on variations in surface characteristics, including the vegetation fraction/index (Gallo et al., 1993). Additionally, Kawashima et al. (2000) has shown a strong linear relationship between the minimum air temperature and NDVI. Therefore, another important goal of this study was to examine the relative role of environmental and instrument-related factors in controlling correlation levels between point observations of T_a and spatially aggregated

---

^{2}The 5 km^2 symbolic notation for the pixel resolution is used to denote a 5 × 5 km^2 pixel.

LST data. The LAI and vegetation fraction, cover type, and MODIS instrument view angle and aggregation scale were among these factors (Campbell and Norman, 1998). Numerous previous studies have shown that distribution of remotely sensed LST at 1.0 km² resolution is highly correlated with vegetation fraction and cover density/greenness measured in terms of NDVI over the regions having typical extent of several hundred kilometers (Price, 1990; Hope et al., 2005). An empirical approach in conjunction with simple analytical estimates was applied for the sensitivity analysis of T_a-LST relationship to these factors. Results of this sensitivity study are also critical for an adequate interpretation of satellite-derived LST data, in particular, when performing analysis of inter-annual variability of LST sets to assess the climate change (Jin and Dickinson, 2002).

This study was performed over an area spanning 4.0° in longitude and 5.5° in latitude, encompassing the entire state of Mississippi and small parts of adjacent states' territories. Both *in situ* surface observations of the air temperature and MODIS LST data were selected for the period from June 2000 to the end of 2004. Obtaining T_a values from LST data using a linear regression between them is a rather simple and straightforward procedure that has been well described in detail in numerous previous studies (e.g., Kawashima et al. 2000). Both T_a and T_s are involved in the surface energy equation (Garratt, 1992) that can be used for analytical estimates of an expected relationship between them. An example of such estimates was documented by Gao (1995), and was used in this study. Another attractive feature of the surface energy equation is that it can be applied for spatial interpolation of involved terms or variables (Gash, 1987).

METHODS

Surface Observations

Observations of daily maximum and minimum air temperature at 161 surface stations were used to assess statistical relationships between T_a and LST values at station locations. The validated surface meteorological data for these stations were obtained from the National Climatic Data Center (NCDC) online archive (NOAA NCDC, 2004). The study area and locations of the chosen stations are shown in Figure 1. The air temperature values refer to the observation height (approximately 1.5 m above ground), often called shelter height. Of 161 selected stations, approximately 30 were reporting T_a hourly and were used in this study.

MODIS LST and LAI

Two groups of MODIS LST products with 1.0 km² (fine) and 5.0 km² (coarse) resolutions were used. They represent current validated version (v004) and were available globally at approximately 10:30 AM/PM (Terra) and 1:30 AM/PM (Aqua) local solar time. Table 1 provides a summary of the MODIS LST products used. Two basic approaches were adopted for retrieving LST from TIR MODIS clear-sky measurements: a generalized split window algorithm for fine resolution (Wan and Dozier, 1996) and a physics-based day/night method (Wan and Li, 1997) for coarse-resolution data was applied. The physical basis of both MODIS LST retrieving algorithms has
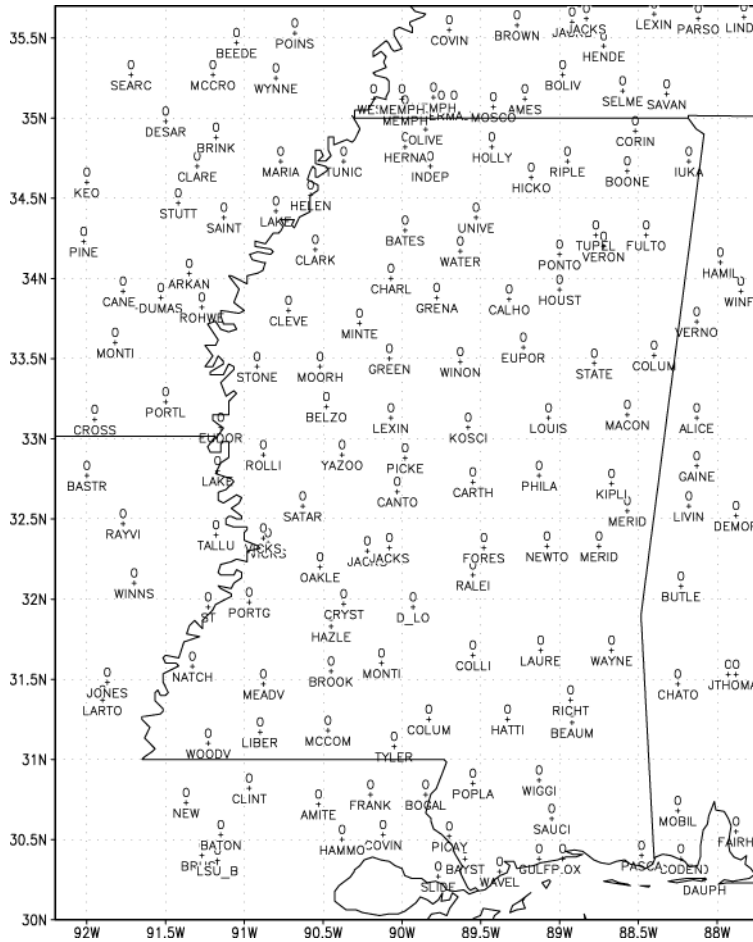
Fig. 1. Geographical distribution of the surface observation points.

Table 1. Summary of the LST MODIS Products Used in This Study

Product name	Algorithm	Nominal accuracy	Pixel/mesh resolution	MODIS TIR band no.
MOD11A1 (Terra)	Generalized split-window	±1 K	1×1 km^2	31 and 32
MYD11A1 (Aqua)	(Wan and Dozier, 1996)			
MOD11C1 (Terra)[a]	Physics-based day/night method	±1 K	0.05° × 0.05° latitude-longitude cell	20, 22, 23, 29, and 31-33
MYD11C1 (Aqua)[b]	(Wan and Li, 1997)			

[a]Based on MOD11B1 5 km resolution LST.
[b]Based on MYD11B1 5 km resolution LST.

been described in detail by Wan (1999). The MODIS LST HDF-files (MODIS, 2001) were downloaded from the Land Processes Distributed Active Archive Center (LP DAAC). Terra files were available from June 2000 and Aqua files from July 2002.

The split-window method described by Wan and Dozier (1996) requires measurements from two TIR bands; the surface emissivity, ε, is assumed to be known at every 1.0 km^2 pixel, and it is specified from the land-cover type data that is based on the MODIS land product (MOD12C1). The *a priori* knowledge of the land-cover type classification—based ε is essential for the accurate retrieval of LSTs. This database for ε relies on homogeneity of the surface properties within the pixel. In many cases, the actual surface of the 1.0 km^2 pixel exhibits a certain heterogeneity; therefore, as noted by Wan et al. (2004), errors might occur in specifying ε from land cover types, especially in arid and semi-arid areas, where overestimates of ε are often observed. The same authors indicated that another source of uncertainty in the application of the split-window algorithm was a deficiency of understanding the emissivity variations with the instrument view angle. Testing results of this algorithm showed that the accuracy of LST estimate was less than 1°K over homogeneous surfaces such as water, crop, and grassland surfaces (Wan et al., 2004).

A pair of daytime and nighttime MODIS coarse-resolution measurements taken under clear-sky conditions in seven TIR bands has been used in the physics-based day/night algorithm for retrieving both LSTs and surface emissivities (Wan and Li, 1997). The algorithm involved a solution of 14 nonlinear equations, and the whole range of the MODIS instrument zenith view angle (0°–65°) was binned into five unequal intervals[3] to represent a view-angle dependence of ε. The physics-based method also showed remarkable performance with a typical LST accuracy of 1°K over homogeneous surfaces and an increase in uncertainty of LST estimates when substantial variations of temperature occurred within 5.0 km^2 pixel.

Wan et al. (2002), having accounted for the intrinsic features of both algorithms and results of comparisons with *in situ* observations suggested using LST split-window 1.0 km^2 product over water bodies, snow/ice, and densely vegetated surfaces and the 5.0 km^2 LST data retrieved from the physics-based method over bare soil or over surfaces with sparse vegetation. Physical and computational aspects of the above-mentioned algorithms have been subjected to permanent improvement by their authors, and soon a new version (v005) of advanced-quality MODIS LST products will be available for the scientific community. LST products (MOD11C1 and MYD11C1) generated on the regular latitude-longitude grid also assimilate 1.0 km^2 observations over the 5.0 km^2 pixels with missing data, thus providing substantially better spatial and temporal coverage (according to our estimates, it is higher by 25–30% on average) as compared with that of fine- and coarse-resolution LST products only. Here we are primarily interested in the analysis and further utilization of MOD11C1 and MYD11C1 products because they virtually represent 0.05° × 0.05° latitude-longitude averaging/generalization of both resolutions of LST data. For comparison with T_a, LST data have been interpolated to station locations shown in Figure 1. The nearest neighbor and the bilinear interpolators (with weightings inversely proportional to the distance) were used for 1.0 and 5.0 km^2 products, respectively.

---

[3]The interval size diminishes with the view angle, so the largest size corresponds to viewing from the nadir.

The MODIS green LAI product (MOD15A2), represented by eight-day average values with fine-resolution data, was used in this study to estimate the fractional vegetation cover, which also depends on the view zenith angle of the MODIS instrument. The MODIS LAI algorithm is based on the numerical solution of the radiative-transfer equation (Knyazikhin et al., 1998). Depending on the input surface spectral reflectance and on their uncertainties and on the vegetation canopy type (biome), results of the solution are organized in the form of look-up tables that provide efficient basis for retrieving LAI fields. Only six biome types were used to represent global variability of vegetation cover corresponding to 1.0 km^2 resolution. A preliminary study of MODIS LAI quality has shown the exceptional performance of this product in reproducing spatially averaged LAI estimates generated from independent high-resolution (30 m) measurements (Myneni et al., 2002). Because of the heterogeneous nature of fine-resolution pixels (they often contain more than one vegetation class), an adequate aggregation of sub-pixel variability represents an attractive property of the current MODIS LAI algorithm.

Also, because the definition of the fractional vegetation cover depends on the vegetation density and how it is distributed within the pixel (Gutman and Ignatov, 1998), the LAI and the vegetation fraction are not completely independent parameters (Carlson and Ripley, 1997). This nontrivial topic requires special consideration, which is beyond the scope of the present paper. Details of LAI dependence on the scale ranging from 1.0 km to 64 km and heterogeneity of a pixel have been published by Tian et al. (2002). Although it was more common to estimate fractional vegetation cover from NDVI, here we have used MODIS LAI for this purpose (Gallo and Daughtry, 1987; Wittich and Hansing, 1995; Gutman and Ignatov, 1998; Zeng et al., 2000). This approach was adopted because it facilitated an interpretation of view-angle-dependent LST measurements representing the TIR signal as a superposition of the vegetation component and a corresponding part originating from the background soil. View-angle-dependent estimates of the vegetation fraction from LAI are readily accepted by the research community, especially over completely vegetated canopies (Campbell and Norman, 1998; Friedl, 2002). Estimates of the vegetation fraction from NDVI and LAI should produce similar results if the view zenith angle of the TIR sensor is close to the nadir and both estimates represent only an approximate measure of ground truth.

Energy Balance of the Surface and ($T_a - T_s$) Difference

The difference between T_a and T_s ($\Delta = T_a - T_s$) represents an important parameter of regional climate, which controls the partition of available energy flux, mainly represented by net solar radiation (Rn), between sensible heat and other fluxes within the surface layer. Also, it can be considered as a footprint influenced by other surface parameters such as albedo, roughness, vegetation canopy type, and soil physical properties. All of these parameters, including delta temperature, are interrelated through a fundamental energy conservation law applied for the surface layer, known as the surface energy balance (Oke, 1987). Therefore, before performing a statistical analysis between T_a and T_s, it would be instructive to consider Δ estimates from the surface balance equation and then use these estimates as a guideline for the interpretation of

correlation/regression features between T_a and T_s. The surface energy equation can be written as:

$$R_n + R_l - \varepsilon\sigma T_s^4 = H + LE + G, \tag{1}$$

where H and LE are vertical turbulent fluxes of sensible and latent heat, respectively, R_l is the downward flux of longwave radiation, ε is the emissivity of the surface, σ is the Stefan-Boltzmann constant, and G is the soil heat flux. At least two basic approaches can be applied for estimating H and LE turbulent fluxes within the ABL containing a vegetation canopy. One is known as a bulk method that relates sensible heat flux to Δ and represents a rather simple modeling approach describing the vertical transfer of energy without partitioning of H and LE fluxes into specific land surface cover types. This approach represents the local surface area as one element, implying an implicit aggregation of various surface components over that area. The method is known as the bulk approach and has been successfully adopted by Voogt and Grimmond (2000) for the modeling of urban heat fluxes.

A more advanced methodology known as SVAT, which describes the vertical exchange of momentum, heat, and moisture and accounts for the local horizontal heterogeneity within ABL, also could be applied. SVAT modeling involves locally explicit and separate consideration of various types of vegetation and soil/land surfaces; although it includes numerous external adjustable parameters (and sometimes it is very difficult to specify them accurately) describing physical properties of vegetation and land/soil. Numerous useful simplifications of SVAT models have been also suggested to assimilate remotely sensed atmospheric and land parameters (e.g., Friedl 1995; Houborg and Soegaard, 2004).

Bulk Approach

The bulk procedure for describing momentum and heat vertical fluxes is relevant and beneficial when the nature of the problem under study does not require an independent consideration of vegetation and bare land surfaces at involved spatial scales. For example, the vertical sensible heat flux can be expressed as follows (Garratt, 1992; Sun et al., 1999; Mahrt and Vickers, 2004):

$$\frac{H}{\rho C_p} = -C_H(Ri, z, z_{0m}, z_{0h})U(z)[T_a - T_0], \tag{2}$$

where C_H is the exchange coefficient for heat at level z where observations of the wind speed U and T_a are available, T_0 is the air temperature close to the surface at level z_{0h} that is the roughness length for heat, ρ is the air density, C_p is the specific heat of air at constant pressure, Ri is the bulk Richardson number for the surface ABL, and z_{0m} is the roughness length for momentum. The coefficient C_H can be evaluated analytically from the universal approximations suggested by Louis (1979) to an accurate but not analytical description of C_H from the ABL similarity theory (Garratt, 1992) for a given set of Ri, z, z_{0m}, and z_{0h} parameters.

For the purpose of H estimating from remotely sensed T_s data, the equation (2) can be simply accommodated as (Sun and Mahrt, 1995):

$$\frac{H}{\rho C_p} = -C_{HR} \, U(z)\Delta, \qquad (3)$$

where C_{HR} is the radiometric exchange coefficient that accounts for substitution of T_0 by T_s in the expression (2). It is important to note that unlike C_H, the coefficient C_{HR} cannot be evaluated from the universal ABL functions involving Ri, z, z_{0m}, and z_{0h} parameters (Sun and Mahrt, 1995).

Using a linear empirical relationship between G and R_n ($G = \beta R_n$, where β is an empirical constant), expression (3), and first-order Taylor approximation for the T_s^4 term, the energy balance of the surface can be rewritten as:

$$R_s \, (1-\beta)(1-a) + R_l - \varepsilon\sigma \, (T_a^4 + 4 \, T_a^3\Delta) = LE - \rho C_p \, C_{HR} \, U(z)\Delta, \qquad (4)$$

where R_s is the solar radiation flux at the surface and a is the surface albedo. The temperature in the surface balance should be expressed in Kelvin. A similar, but more general, approach was developed by Gao (1995) mainly for T_a assessment, using satellite observations for the remaining terms/variables involved in the balance. He used a second-order Taylor approximation both for T_s^4 and LE terms and assumed a saturation condition for the water vapor at the surface having temperature T_s. A universal application of this condition could be questioned because it is certainly valid for specific surface types only; therefore, we did not apply a Taylor expansion for the LE term.

For a given set of R_s, LE, and other terms, equation (4) can be used to estimate the difference between air and surface temperatures (Δ). Under clear skies, radiation energy components (R_s and R_l) vary gradually and rather slowly in space as compared with LE component, a, T_s, and wind speed variables, which typically can experience quick and sharp changes over relatively small distances of about 1.0 km. These sudden changes are modulated by corresponding spatial variations of the surface's physical properties depending on soil moisture, vegetation cover type, and surface roughness and shape alternations that can be traced very effectively by remote sensing instruments. The magnitude of Δ is controlled by the positive difference between $R_s(1-a)$ and LE over mid-latitude/subtropical grasslands (Brutsaert, 1982) during late morning and early afternoon hours. Other terms in equation (4) produced substantially minor impacts on Δ. With this simplification, it is almost clear that one can expect a linear relationship between T_a and T_s temperatures from equation (4) in the following form: $T_a = T_s + const$, having the slope equal to one. Indeed, as it will be shown further, empirical relationships between T_a and T_s manifest the slope, which is approximately equal to one (Figs. 3–5). Equation (4) essentially describes the surface energy budget of a point size (Friedl, 2002), implying a horizontal homogeneity within ABL/vegetation and underlying soil columns. Applying the equation with remotely sensed LSTs required a spatial averaging to provide pixel-aggregated estimates of T_s.

Averaging Effects

A spatial averaging of the non-linear elements produces additional terms proportional to covariations between variables involved (Equation 4). Because the main goal of this section is to illustrate qualitatively the effect of averaging, symbolic forms for *LE* and *G* terms are retained for the sake of simplicity. The use of usual gradient-flux forms for these terms will only result in additional covariations between variables involved in them. Before performing this averaging, a minor simplification of the equation was adopted. Considering that the R_l (which is proportional to T_a^4) and $\varepsilon\sigma T_a^4$ terms are relatively small during the daytime as compared to the difference between the net radiation and *LE* terms and almost cancel each other, the above two small terms may be omitted. Using the notation $F = R_s(1-\beta)(1-a) - LE$, assuming that C_{HR} is a constant and neglecting a very small covariation between R_s and albedo *a*, the simplified, spatially averaged surface energy budget can be written as follows:

$$\bar{F} \approx 4\varepsilon\sigma[\bar{T}_a^3\bar{\Delta} + 3\bar{T}_a^2(\overline{T_a'\Delta'})] - \rho C_p C_{HR}[\bar{U}(z)\bar{\Delta} + \overline{U'(z)\Delta'}], \tag{5}$$

where the overbar denotes a spatial average and a prime stands for a deviation from this average. It is essential to understand that the averaged surface budget accounts for a spatial aggregation of remotely sensed T_s (Friedl, 2002). The aggregation/averaging scale can be represented by both data resolutions of the MODIS LST.

The covariation term involving temperatures $(\overline{T_a'\Delta'})$ is typically smaller than the corresponding mean component $\bar{T}_a\bar{\Delta}$, because, in general, $\bar{T}_a \gg T_a'$ ($\bar{T}_a$ is about 280–300 K and T_a' is in the range 5–10 K usually) and $\bar{\Delta}$ has the same order as Δ'. Conversely, covariations involving the wind speed $U'(z)\Delta'$ have values that can be as large as those of the mean term $\bar{U}(z)\bar{\Delta}$ because the wind speed deviation $U'(z)$ and $\bar{U}(z)$ typically are of the same magnitude. Previous studies have not considered these covariations (Gao, 1995, Friedl 2002; Caparrini et al., 2003). Equation 5 shows that the average difference between temperatures $\bar{\Delta}$ is controlled not only by the mean fields of $\bar{T}_a$, $\bar{T}_s$ and $\bar{U}(z)$, but also depends on spatial statistics including covariations of these variables.

The covariation term $(\overline{T_a'\Delta'})$ has a particular significance because it can be rewritten as $\sigma_a^2 - \rho_{as}$, where $\sigma_a^2 = \overline{T_a'^2}$ is the variance of the air temperature and $\rho_{as} = \overline{T_a'T_s'}$ denotes the covariation between T_a and T_s, thus providing a framework for ρ_{as} or correlation estimation from the averaged energy budget (Equation 5). The equation can be readily used for ρ_{as} evaluation at any arbitrary moment of time, *t*. Furthermore, it is easy to relate ρ_{as} to covariations between both T_a^{max} and T_a^{min} with T_s. Another (empirical) way to estimate the correlation coefficient *R* between T_a and T_s temperatures (*R* is defined as the value of ρ_{as} normalized by standard deviations of T_a and T_s) is considered in the next section of this paper.

Considering that the spatial deviations T_a' and T_s' are interrelated as follows $T_s' = -\sigma_0 T_a'$ (Gao, 1995), it is possible to rewrite the covariation $(\overline{T_a'\Delta'})$ as $\alpha_a^2(1-\alpha_0)$. Here $\alpha_0 = 1/\alpha_T$ and α_T is the temperature transfer coefficient reflecting a decreasing rate of the temperature spatial deviations with height. This coefficient may vary in the range of 0.45–0.95 (Gao, 1995), increasing with surface roughness and decaying with the observation height *z*. Bearing in mind the above relation between T_a' and T_s', one

can compare the covariation term with the mean temperature term $\overline{T}_a^3 \overline{\Delta}$. After minor rearrangements, the ratio between these terms can be expressed as $3 \sigma^2_a(1 - \alpha_0)/(\overline{T}_a \overline{\Delta})$. This ratio is proven to be less than 0.01 (or 1%) for given typical values of involved quantities ($\alpha_T = 0.9$, $\sigma_a = 2.25$ K, $\overline{T}_a = 290$ K, and $\overline{\Delta} = 5$ K). This result indicates that the temperature covariation term has an overall negligible impact on the spatially averaged surface energy budget. Also, the spatial derivatives of this covariation term might be as large as those of the mean temperature term. These spatial derivatives of the terms involved in the surface energy balance in Equation 5 have been used in the interpolation routines (Gash, 1987).

RESULTS

Plots of daily maximum and minimum T_a show a relatively high day-to-day variability of these temperatures exceeding in the average 15ºC during a period from October to May (data not shown). This variability is apparently associated with the passage of cold fronts through the study area with a characteristic periodicity in the range of 6–12 days. Conversely, a lower day-to-day variability with related changes not exceeding 6–8ºC is manifested during the June–August period. These relatively low air temperature variations are modulated primarily by precipitation and/or cloud cover changes. Cold fronts could affect the study area during late June or August, although generally there is no sharp temperature change associated with the atmospheric fronts in this season. A joint analysis of T_a and T_s plots at selected locations over the state of Mississippi demonstrated a rather close agreement between them, indicating that MODIS LST can mimic observed day-to-day air temperature variability reasonably well, especially for the October–May "cold" season and the minimum temperature. This fact represents necessary empirical background for the current study and supports use of linear regression models to produce adequate estimates of T_a temporal variations from the MODIS LST.

Figure 2 shows examples for clear-sky diurnal variations of the normalized air temperature defined as $(T_a - T_a^{min})/(T_a^{max} - T_a^{min})$, where T_a^{min} and T_a^{max} are the daily minimum and maximum air temperatures, respectively. A regular diurnal cycle of the normalized temperature is evident, with a rather strong association between air normalized temperature at Terra and Aqua overpass time intervals shown as vertical dashed lines and corresponding values of T_a^{min} and T_a^{max}. Figure 2 explains the general idea for regression estimation of T_a^{min} and T_a^{max} from remote LST measurements, provided that LST and air temperature at satellite overpass time are strongly related.

Diurnal Cycle and Aggregation Scale

Terra satellite overpass time, t_0 (both AM and PM), may differ from the time when the daily maximum or minimum of the air temperature occurs. Thus, the impact of this time difference must be assessed, roughly estimated as 3 h for T_a^{max} and 8 h for T_a^{min}, on linear regression estimates of T_a^{max} and T_a^{min} from T_a. Scatterplots shown in Figure 3 illustrate how closely T_a sampled at t_0 is related to T_a^{max} and T_a^{min} using air temperature observations at Tupelo Regional Airport (AP) during 2000–2004. To provide homogeneity of meteorological conditions and thus better comparability between different dates, only measurements under all day/night clear-sky conditions
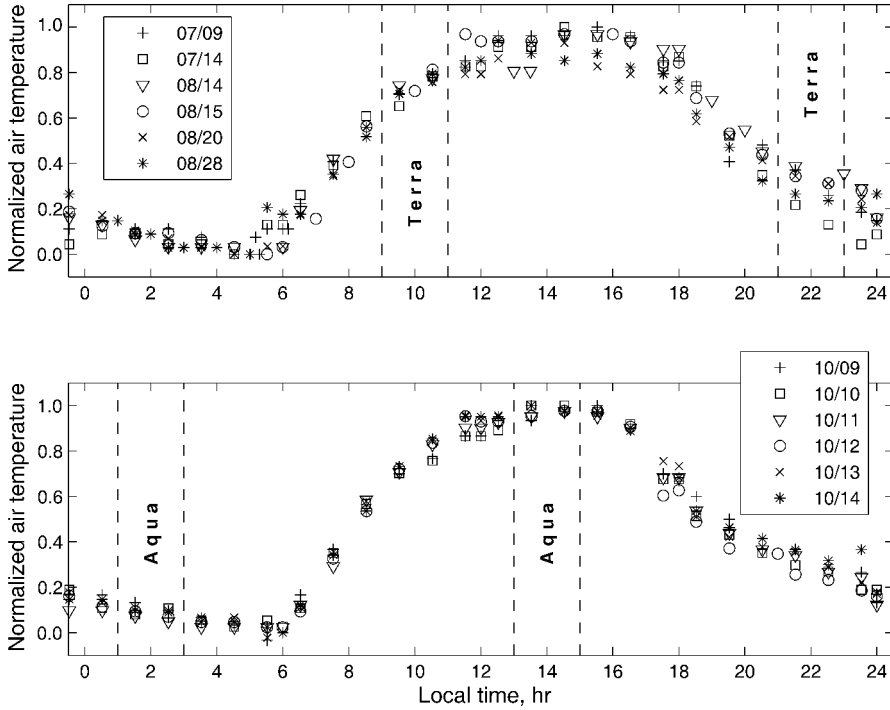
Fig. 2. Daily cycle examples of normalized air temperature observed at Tupelo Regional Airport, Mississippi during clear-sky days/nights covering summer–fall period of 2000. Vertical dashed lines represent Terra overpass time interval (upper frame) and that of for Aqua (lower frame).

were used in Figure 3. Partly cloudy or overcast weather will result in distortion of the relatively regular diurnal cycle of T_a, illustrated in Figure 2, leading to additional scatter between temperatures plotted in Figure 3. The above estimates of the relationship between the air temperature sampled at t_0 and its maximum or minimum daily values might be considered as an ideal regression supposing that T_a could be retrieved by satellite with perfect accuracy and neglecting potential deviations of the air temperature between *in situ* point surface measurements and area-averaged satellite data. Plots presented in Figure 3 indicate that even in these ideal conditions there is a noticeable scatter between T_a sampled at satellite AM/PM overpass time and daily maximum/minimum air temperature. This scatter can be evaluated as a standard deviation or σ of $\Delta_{max} = T_a^{max} - T_a$ (10:30 AM) and of $\Delta_{min} = T_a^{min} - T_a$ (10:30 PM).

These ideal/expected relationships represent reference regression cases. Closer agreement and less scatter (σ is about 1°C on average) are observed between T_a selected at 10:30 AM and T_a^{max}, reflecting a smaller time span of about 3 hours between observation times for these variables, than between T_a sampled at 10:30 PM and T_a^{min} (the σ value of Δ_{min} exceeds 2°C), as is plainly depicted in Figure 3 and Table 2. This Table also shows (both for the Terra and Aqua platforms and for different spatial resolutions) other relevant statistics for T_a^{max} versus LST and T_a at 10:30 AM and T_a^{min} versus LST and T_a at 10:30 PM, including the correlation coefficient
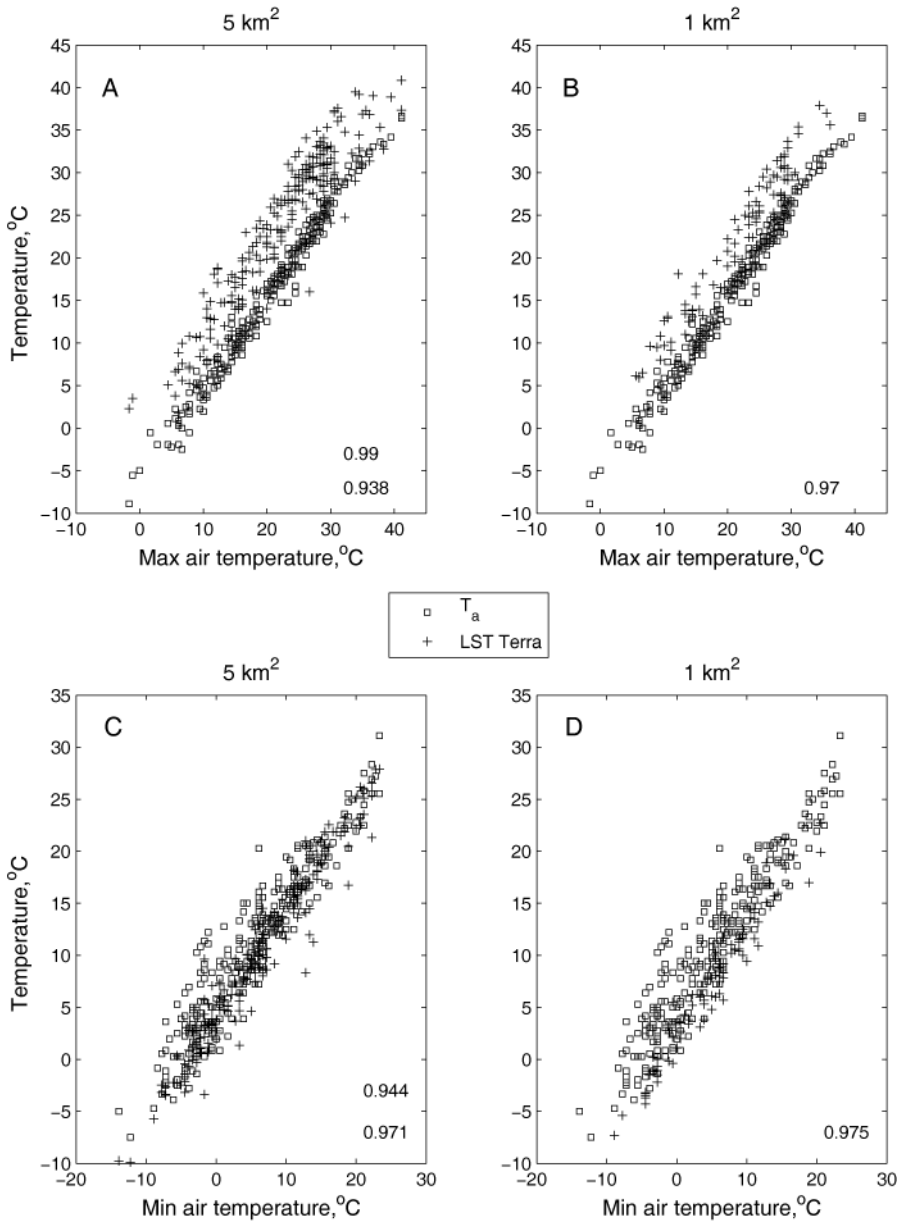
Fig. 3. Scatterplots between observed air temperature for Tupelo Regional Airport, Mississippi at 10:30 AM and daily maximum (A, B) and between observed T_a at 10:30 PM and daily minimum temperature (C, D) are shown by squares. Crosses indicate relationships between MODIS Terra LST measured around 10:30 AM and T_a^{max} (A, B) and LST around 10:30 PM and T_a^{min} (C, D). Left (A, C) and right (B, D) frames depict global MODIS Terra LST data with 0.05° latitude-longitude resolution (approximately 5.0 km²) and 1.0 km² resolution, respectively. Correlation coefficients are depicted in lower right corners (upper row value stands for correlation between air temperatures, and lower row—for correlation between T_a and LST).

(R) and the mean value. Note that R values reflect the strength of the linear relationship between temperature variables.

The elevated level of point scattering for the $T_a\text{min} - T_a$ relationship is mainly attributed to significant variations of T_a values observed around 10:30 PM (Fig. 2). As can be expected, similar plots created for Aqua overpass time (1:30 PM and 1:30 AM), which is very close to the $T_a\text{max}$ and $T_a\text{min}$ observation time (Fig. 2B), produce substantially less scatter between T_a and its daily maximum and minimum values (with σ values of 0.63°C and 1.32°C, respectively), particularly between T_a sampled at 1:30 PM and $T_a\text{max}$ (Fig. 4 and Table 2). Comparing the performance of this ideal regression for both platforms, one cannot but infer that Aqua LST fields provide better results than those of Terra. Indeed, the σ values for Δ_{max} decrease about twofold in value from 1.46°C to 0.63°C and from 2.67°C to 1.32°C. Note that σ value of Δ is a general measure of scattering between variables (in the above case they are T_a, $T_a\text{max}$, and $T_a\text{min}$) involved in the regression. Clearly lower values of σ result in more accurate regression estimates.

Similar scatterplots were also generated to evaluate regression performance between MODIS LST and daily $T_a\text{max}$ and $T_a\text{min}$. Crosses in Figure 3 show corresponding relationships between them. It is reasonable to analyze relationships involving $T_a\text{max}$ and $T_a\text{min}$ separately, and at first we consider the $T_a\text{max}$ case. Using Terra late morning overpass LST (with 0.05° × 0.05° latitude-longitude resolution) instead of T_a leads to deterioration of the regression with $T_a\text{max}$. This is mainly manifested in significant lowering of the correlation from 0.99 for $T_a\text{max}$ and T_a pairs to 0.94 and 0.97 for $T_a\text{max}$ and LST pairs at 0.05° latitude-longitude (approximately 5.0 km²) and at 1.0 km² resolution, respectively. Using the LST instead of T_a also results in increasing the standard deviation of Δ_{max} from 1.46°C to 3.12°C for 5.0 km² and to 2.09°C for 1.0 km² resolution (Table 2). There is no escape from the conclusion that LSTs with 1.0 km² resolution are in better and closer agreement with $T_a\text{max}$ in terms of higher R and lower standard deviations as compared with those of the 5.0 km² LST product. This conclusion is also valid for the Aqua LST product (Table 2 and Figs. 4A–4B). Unlike the ideal regression case between $T_a\text{max}$ and T_a at 10:30 AM, a change from the Terra to the Aqua platform while using LST in place of T_a does not lead to a regression improvement for both data resolutions. Corresponding changes in R remain insignificant at the 95% significance level and σ values remain at the same level as is shown on the left side of Table 2.

The results reported in this section reflect relationships between temperatures under clear-sky conditions (whole daily cycle of T_a) only. These results may change if we relax all-day clear-sky sampling and select a broader sample of temperatures, permitting cloudiness to be present between MODIS overpass times. Therefore, R and standard deviations were recalculated for all cases with available LST observations. For convenience we refer to these results as a sample A, which is highlighted in Table 2. MODIS LST products are retrieved under clear skies, implying only a negligible amount of clouds present within a MODIS pixel at the overpass time, and certainly some cloudiness may exist at the time of observed daily $T_a\text{max}$ and $T_a\text{min}$. Additionally, one more estimate of R and standard deviation (B results) based on a selection of cloud-free conditions using a 1.5 h time-window around the MODIS overpass time and utilizing hourly *in situ* observations of cloudiness fraction were

Table 2. Correlation Coefficient (R) between $T_a(max/min)$ and LST (or T_a)[a]

MODIS observation time	Parameter	Pixel size, km	T_a^{max}				T_a^{min}			
			R	$R_{low/up}$	Mean Δ, °C	$σ_Δ$, °C	R	$R_{low/up}$	Mean Δ, °C	$σ_Δ$, °C
10:30 AM/ PM	T_a	Point	0.990	0.988 0.992	4.65	1.46	0.944	0.929 0.955	-5.62	2.67
			0.990	**0.988 0.991**		**1.55**	**0.961**	**0.956 0.966**		**2.65**
	LST (*Terra*)	5	0.938	0.921 0.952	-1.58	3.12	0.971	0.962 0.978	-4.04	1.89
			0.874	0.857	0.55	4.34	0.923	0.913	-2.53	3.44
			0.928	**0.888**		**3.41**	**0.899**	**0.932**		**4.13**
		1	0.970	0.954 0.980	-0.73	2.09	0.975	0.962 0.983	-2.10	1.47
			0.972	0.962	-0.81	2.17	0.961	0.949	-1.64	2.07
			0.969	**0.979**		**2.20**	**0.970**	**0.970**		**1.73**
1:30 PM/ AM	T_a	point	0.998	0.997 0.998	1.08	0.63	0.986	0.983 0.989	-2.48	1.32
			0.997	**0.996 0.997**		**0.79**	**0.989**	**0.987 0.990**		**2.07**
	LST (*Aqua*)	5	0.914	0.880 0.939	-3.63	3.54	0.977	0.966 0.984	-2.60	1.68
			0.848	0.823	-1.13	4.58	0.900	0.882	-1.22	3.80
			0.913	**0.870**		**3.56**	**0.857**	**0.916**		**4.25**
		1	0.968	0.935 0.984	-3.18	2.24	0.989	0.979 0.994	-0.81	0.97
			0.960	0.937	-2.63	2.52	0.973	0.958	-0.93	1.49
			0.963	**0.975**		**2.34**	**0.977**	**0.982**		**1.25**

[a]$R_{low/up}$ are lower and upper bounds of 95% confidence interval for R. Mean and standard deviation (σ) of $Δ = Ta(max/min)$ – LST (or T_a). Statistics are estimated for all-day clear-sky (CLR) and for any cloudiness conditions (grey shading), including CLR during day/night at Tupelo Regional Airport. Note that MODIS LST is available only under CLR or almost-CLR conditions, implying at least a negligible amount of clouds present within a MODIS pixel at observation time. Bold values indicate statistics sampled for CLR within the 1.5 h time-window around the MODIS observation time.

performed (Table 2). Variations of R and σ between A and B samples are attributed to a difference among *in situ* observed and MODIS-related cloud-free definition.

Comparing R and σ of the ideal regression results for T_a^{max} between all-day clear skies and B sampling, one can conclude that observed variations of cloudiness between MODIS overpass times have little effect on the regression performance. There are no statistically significant changes in R (Table 2). Similarly, only slight
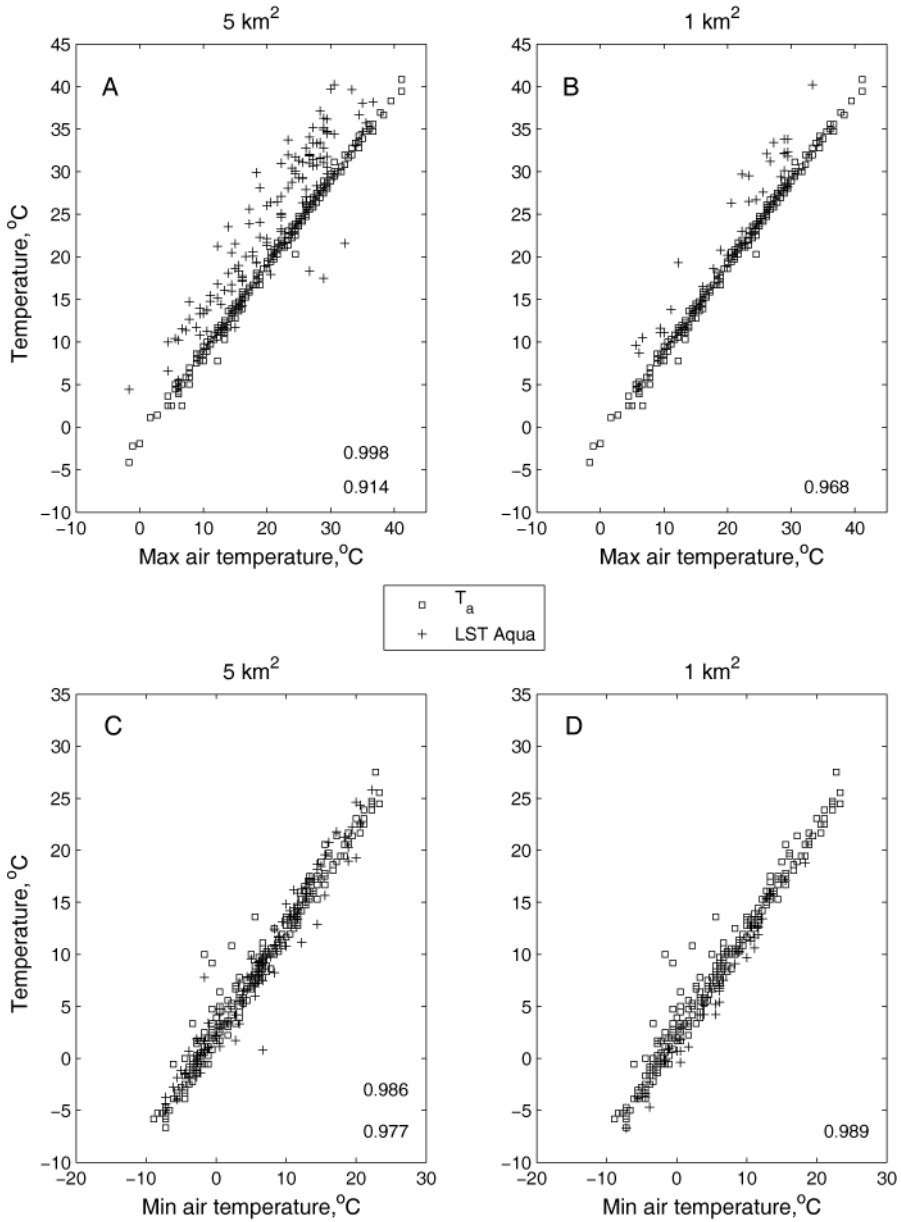
Fig. 4. Scatterplots between observed air temperature for Tupelo Regional Airport, Mississippi at 1:30 AM and daily maximum (A, B) and between observed T_a at 1:30 PM and daily minimum temperature (C, D) are shown by squares. Crosses indicate relationships between MODIS Aqua LST measured around 1:30 AM and T_a^{max} (A, B) and LST around 1:30 PM and T_a^{min} (C, D). Left (A, C) and right (B, D) frames stand for global MODIS Aqua LST data with 0.05° latitude-longitude resolution (approximately 5.0 km²) and 1.0 km² resolution, respectively. Legend for correlation values is explained in Figure 3.

Table 3. Correlation Coefficient R between $T_a(max/min)$ and T_s, for Different Combinations of Land Cover Types and Seasons[a]

Land cover types	Statistic	R_{max}		R_{min}	
		May–Sept.	Oct.–Apr.	May–Sept.	Oct.–Apr.
Crops and grasslands	Mean	0.68	0.85	0.91	0.90
	σ	0.13	0.05	0.03	0.04
Forests	Mean	0.73	0.84	0.91	0.90
	σ	0.09	0.04	0.08	0.05

[a]σ values indicate standard deviation of R. The sample size is the same as in Table 4.

reductions in R and increase of σ values occur when we change from clear-sky to B sampling for the regression between T_a^{max} and LST at both resolution. Conversely, both the Terra and Aqua data show a dramatic lowering of R and increasing σ values, which are observed for the T_a^{max}/LST pair when sampling strategy A has been used at 5.0 km[2] resolution (Table 2). Therefore, sampling LST at MODIS 10:30 AM overpass time based on cloud-free conditions inferred from *in situ* surface observations can significantly improve original regression estimates between and LST (Table 2).

In contrast to the case of T_a^{max}, an application of night-overpass LST instead of T_a leads to a closer relationship with T_a^{min} and less scatter (Fig. 3C and Table 2). This is particularly distinct for Terra LST, when R increases from 0.94 (ideal T_a^{max} regression) to 0.97 and 0.98 at 5.0 and 1.0 km[2], respectively. All these changes in R are statistically significant at the 95% level, as depicted in Table 2. There are no significant variations in R for the Aqua LST data. Corresponding σ changes demonstrate decreases from 2.67°C (1.32°C) for ideal regression to 1.89°C (1.68°C) and to 1.49°C (0.97°C) for the regression with LST at 1.0 and 5.0 km[2], respectively.[4]

The high level of R values shown in Table 2, which typically exceed a 0.9 threshold, were not an unexpected result, representing mainly seasonally substantial and coherent changes in T_a and LST temperatures. Applying stratification of R for specific seasons results in an overall decrease of correlation coefficient values. At most stations over the study area, R drops on average to as low as 0.6–0.9 (Mostovoy et al., 2005) for season samples at individual points and exhibits marked seasonal variations (Fig. 11 and Table 3). Migration to the lower (32 km[2]) resolution for T_a and T_s data, available every three hours from the North American Regional Reanalysis (NARR) online archive (Mesinger et al., 2004), results in little seasonal variability of point correlation coefficients (Mostovoy et al., 2005). These findings are also confirmed by a similar temperature data analysis at other hourly-reporting locations (Fig. 5).

The above results clearly show that sampling conditions substantially affect T_a^{max} versus Terra or Aqua 5.0 km[2] LST regression performance estimated in terms of R and standard deviation values. They change significantly when going from all-day cloud-free to LST sampling (A sampling), leading to a marked deterioration of the regression. The LST sampling based on the surface *in situ* observations of the cloudiness (B sampling) leads to closer agreement with the ideal regression. This result

[4]Values in parentheses stand for the statistic based on the Aqua data.
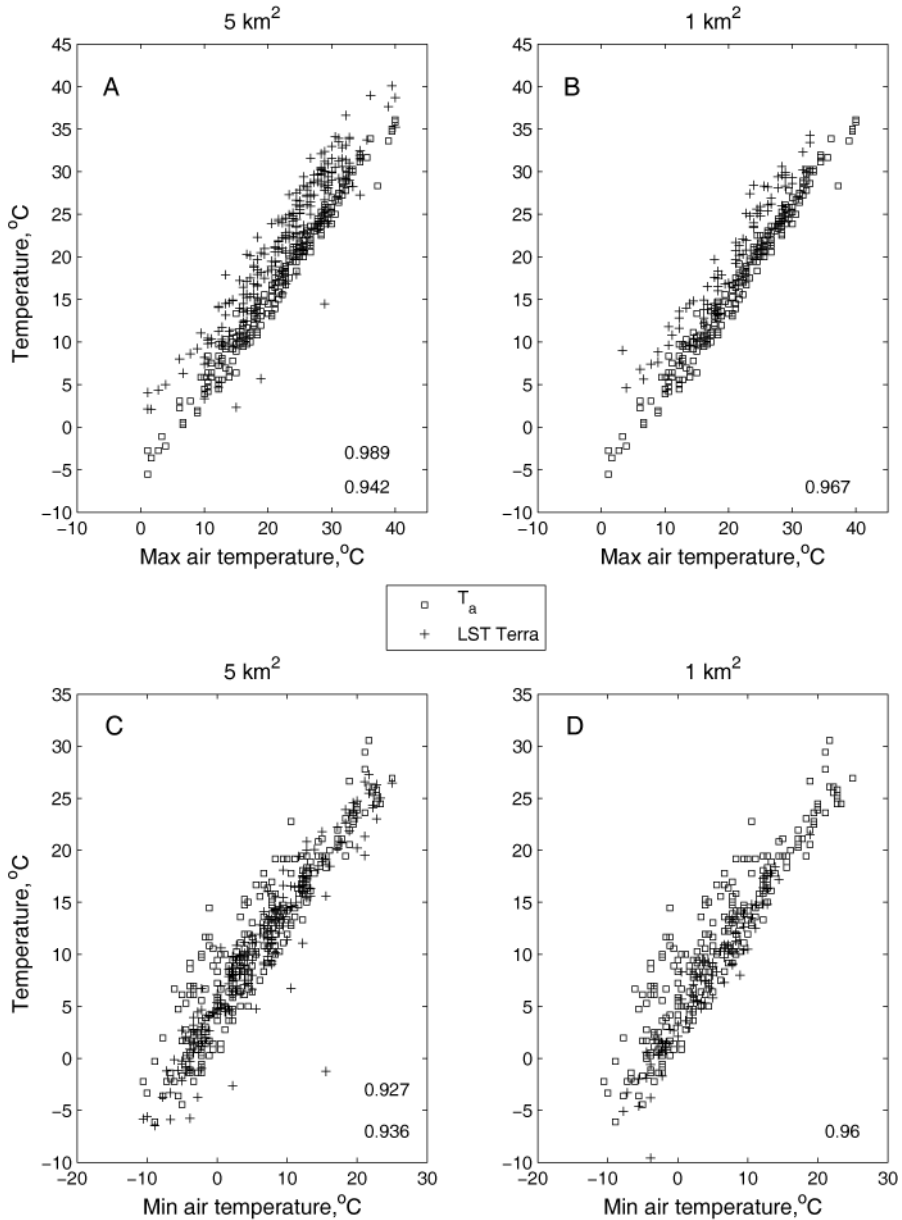
Fig. 5. Scatterplots between observed air temperature for Jackson International Airport, Mississippi at 10:30 AM and daily maximum (A, B) and between observed T_a at 10:30 PM and daily minimum temperature (C, D) are shown by squares. Crosses indicate relationships between MODIS Terra LST measured around 10:30 AM and $T_a$max (A, B) and LST around 10:30 PM and $T_a$min (C, D). Left (A, C) and right (B, D) frames stand for global MODIS Terra LST data with 0.05° latitude-longitude resolution (approximately 5.0 km²) and for 1 km² resolution, respectively. Legend for correlation values is explained in Figure 3.

provides the potential for improvement of $T_a{}^{max}$ regression estimates using 5.0 km² LST data by the appropriate sampling of the clear-sky conditions at MODIS overpass times. In contrast, both the Terra and Aqua 1.0 km² LST products demonstrate that R and σ values are almost insensitive to changes in sampling method. A change from 5.0 to 1.0 km² resolution only slightly improves the overall regression performance between T_a*(max/min)* and LST (Table 2 and Figs. 3 and 4). The relationship between LST and $T_a{}^{min}$ is proven to be closer in terms of higher R values and lower standard deviations as compared with those for $T_a{}^{max}$ regression for both resolutions of Terra data.

View Angle and Vegetation Fraction

The MODIS TIR sensor view zenith angle θ varies between ±65°, and a negative sign of θ means the TIR sensor is viewing the pixel from the east. The angle θ controls the LST value over partially vegetated pixels, since the view angle regulates distribution of the TIR signal between the vegetation and the background soil components. These components usually have different temperatures, and spatial and day-to-day changes of θ over the study area may cause LST variability. Therefore, when performing the regression analysis between T_a and T_s temperatures, it is important to evaluate the potential impact of view-angle variations on regression estimates at a regional scale. First, we consider dependence of Δ_{max} and Δ_{min}, which describe the difference between T_a*(max/min)* and T_s measured at MODIS Terra overpass times upon θ. Although θ typically changes sign for a given pixel every other day, our preliminary study reveals no feasible difference in temperature between two T_s sets sampled for positive and negative view angles. Thus, both positive and negative (substituted by abs(θ)) values of θ are used together in this study.

Neglecting differences in thermal emissivity between bare soil and vegetation and taking into account that both emissivities are close to unity, remotely sensed surface temperature may be expressed as (Norman et al., 1995):

$$T_s^4 (\theta) = (1 - f)T_{s0}^4 + fT_v^4, \tag{6}$$

where T_{s0} is the bare soil temperature and T_v is the vegetation canopy temperature. A fraction of the TIR radiometer field of view $f(\theta)$ occupied by vegetation can be written as (Norman et al., 1995):

$$f(\theta) = 1 - \exp[-0.5LAI/\cos(\theta)]. \tag{7}$$

Equation 7 is valid for the random canopy with a spherical leaf angle distribution that is represented by the extinction coefficient 0.5 in the exponent and predicts an overall growth of f with increasing θ (Campbell and Norman, 1998). The rate of this growth is *LAI* dependent, so that lower values of *LAI* result in higher growth rates of f with view angle. The dashed lines in Figure 6 (A, C) show the $f(\theta)$ function for different *LAI* values (1, 2, and 3); additionally, the function [1- $f(\theta)$] is depicted for *LAI* = 1 and *LAI* = 3 in Figure 6 (B, D). Formulae (6) and (7) describe the dependence of T_s upon a view zenith angle, canopy architecture, and *LAI*. The f value at $\theta = 0$ is known
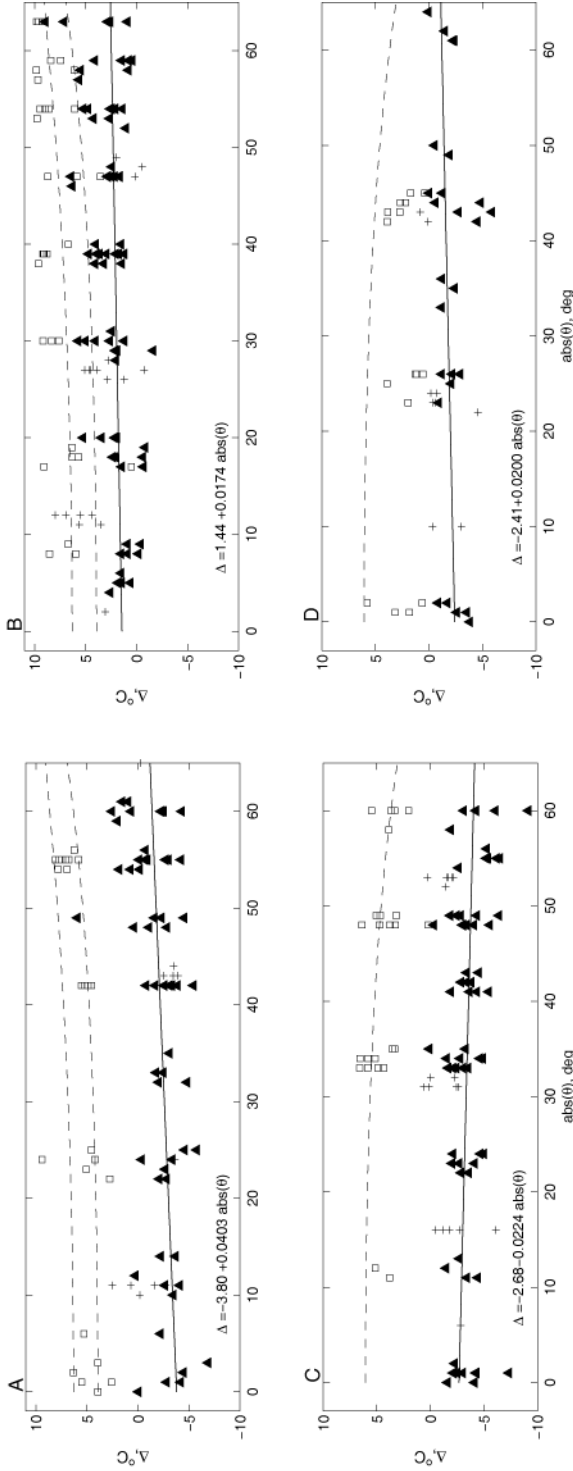
Fig. 6. Relationships for May–Sept. 2000–2004 (A) and (B) between $\Delta = T_a^{\max} - T_s$ and zenith view angle θ; and (C) and (D) between $\Delta = T_a^{\min} - T_s$ and θ. Triangles refer to 5 km T_s data and crosses to 1.0 km^2 data. Scatterplots are shown by squares (A) and (B) between vegetation fraction f and θ; and (C) and (D) between $(1-f)$ and θ. Plotted values of f and $(1-f)$ were multiplied by 10. Dashed lines show θ dependence of f and $(1-f)$ evaluated from expression (7) for different values of AI. A. $LAI = 1$ (lower line) and $LAI = 2$ (upper). B. $LAI = 3$. C and D. $LAI = 1$. Plotted data were selected (A) and (C) at Tupelo Regional Airport, Mississippi; and (B) and (D) at Saucier, Mississippi.

as a vegetation fraction (Norman et al., 1995), but we will use this compact name to denote f in the rest of the paper without regard for the θ value.

During the clear-sky day $T_{s0} > T_v$ usually, so we can assume for simplicity that they are interrelated as follows: $T_s{}^4{}_0 \approx T_v{}^4 + 4T_v{}^3\delta$, where the first-order Taylor expansion for $T_s{}^4{}_0$ is used, and $\delta = T_{s0} - T_v$. Substitution of this relationship results in the following approximate expression for the surface temperature:

$$T_s (\theta) \approx T_v [1 + 4(1 - f) \, \delta/T_v]^{1/4}. \qquad (8)$$

The equation predicts decreasing T_s with the growth of f for a specified constant value of the temperature difference δ between soil and vegetation. For example, if $\delta =$ 5 K, T_v= 290 K and f changes from 0.6 to 0.9 (due to θ variations from 0° to 65°, respectively). T_s measured by TIR at $\theta = 0°$ (as compared with that retrieved at $\theta =$ 65°) decreased by 0.51% (the absolute value of the lowering of T_s is 1.4°C), and increased up to 2.9°C for the larger temperature difference $\delta = 10$ K. Both values represent a significant change in T_s that cannot be ignored when performing T_s spatial analysis or interpolation. Due to daily variations in the surface temperature and difficulties in choosing an appropriate/universal scaling or normalization for this variability, there were no obvious indications of decreasing T_s with increasing θ in MODIS TIR data over the state during day/night hours. The absence of θ dependence in the MODIS LST data is very likely masked by relatively high day-to-day variations of T_s. Typically, during late evening and night hours $\delta \approx 0$ or even less than zero, so θ-dependence of T_s must be weak or nearly absent. Also the equation predicts an increase in TIR-measured surface temperature with θ in case of $\delta < 0$.

Figures 6 and 7 represent scatterplots for Δ and θ at Tupelo (34.27°N, 88.77°W) and Saucier (30.63°N, 89.05°W) for the periods May–September and October–April. Here we adopted the following notation: $\Delta_{max} = T_a{}^{max} - T_s$ (10:30 AM) and $\Delta_{min} = T_a{}^{min} - T_s$ (10:30 PM). These examples clearly demonstrate that, contrary to T_s, Δ reveals rather θ-consistent behavior that correlated well with predictions of T_s from equation (8), so that typically Δ_{max} increase and Δ_{min} slightly decrease or remain constant with the view angle. The LST 5.0 km² resolution data illustrated in Figures 6 and 7 indicate a linear regression relationship between Δ and θ that is obtained by application of the robust least-squares procedure (Holland and Welsch, 1977). This procedure relaxed the influence of outliers in the data upon regression estimates and might be advantageous in the present case of considering noisy LST satellite measurements. Figures 6 and 7 describe f (A, B) or (1-f) (C, D) θ dependence estimated for different values of LAI (Equation 7).

Figure 6 (A, B) illustrates that a positive slope parameter of the regression between Δ_{max} and θ, reflecting an increase of Δ_{max} with the view angle, is dominant during the May–September period. For a given slope parameter value (presented in the lower left corners of the plots in Figure 6) and θ change from 0° to 65°, this increase of Δ_{max} may range from 2.84°C to 1.33°C at Tupelo and Saucier, respectively. The above gradual changes in Δ_{max} are in perfect agreement with θ-related variations of T_s during the daytime, estimated from equation (8) earlier in this section. Histograms of the slope parameter in Figure 9A for all available points over the study area also strongly support the dominance of positive values of this parameter for the May–September period by producing a remarkable shift toward positive numbers.
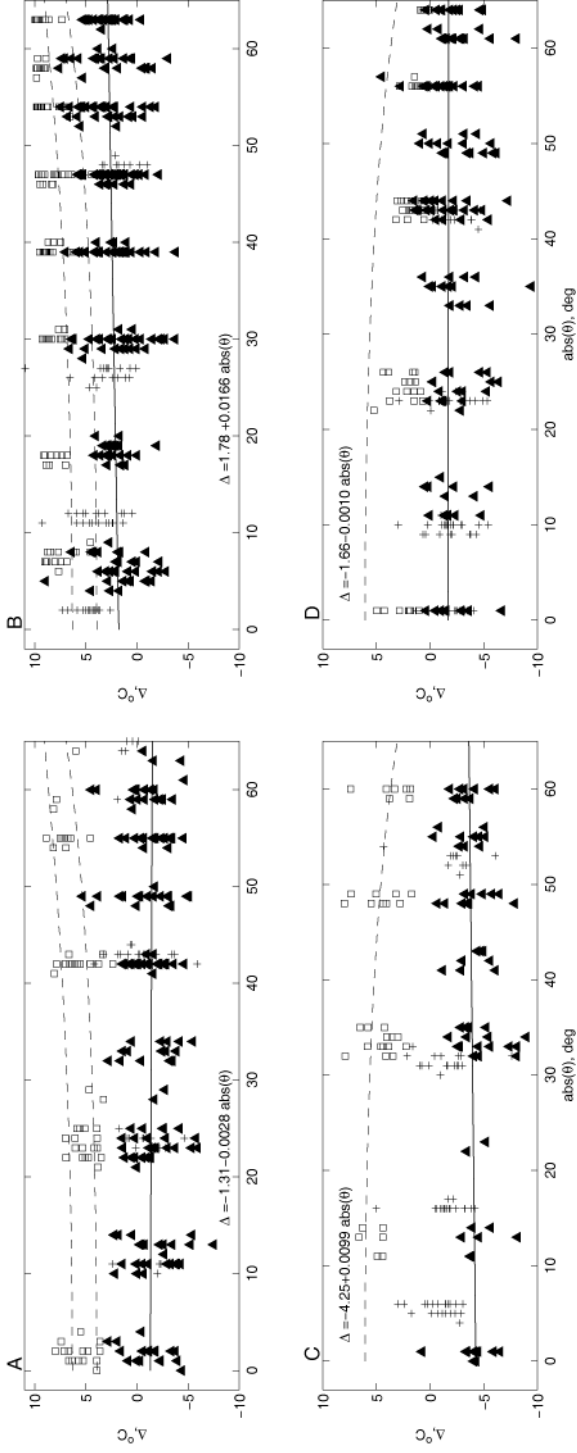
Fig. 7. Relationships for October–April 2000–2004 (A) and (B) between $\Delta = T_a^{\max} - T_s$ and zenith view angle θ; and (C) and (D) between $\Delta = T_a^{\max} - T_s$ and θ. Triangles refer to 5.0 km² T_s data and crosses to 1.0 km² T_s data and squares to 1.0 km². Solid lines stand for least-square approximations of regression between Δ and θ for 5.0 km² data. Scatterplots are shown by squares (A) and (B) between vegetation fraction f and θ: and (C) and (D) between $(1 - f)$ and θ. Plotted values of f and $(1 - f)$ were multiplied by 10. Legend is the same as in Figure 6.
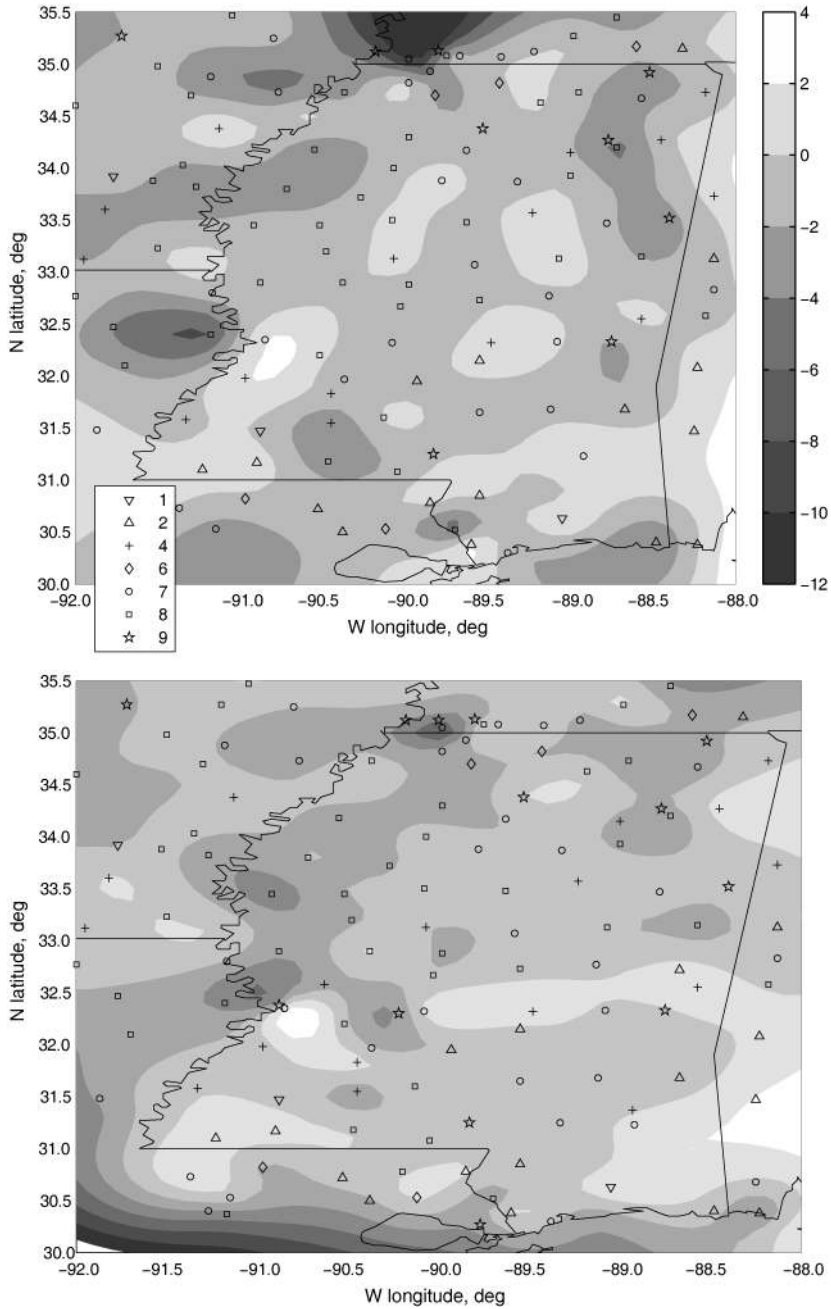
Fig. 8. Geographical distribution of intercept values for the regression between $\Delta_{\max} = T_a^{\max} - T_s$ and view zenith angle. Outputted fields were averaged for May–Sept. (upper frame) and for Oct.–Apr. (lower frame), 2000–2004. Various symbols indicating land cover types show locations where intercept values were estimated as follows: (1) evergreen needle leaf trees; (2) evergreen broadleaf trees; (4) deciduous broadleaf trees; (6) grass; (7) cereal crops; (8) broadleaf crop; and (9) urban and built-up areas.

Table 4. Comparison of $\Delta = T_a(max/min) - T_s$ between Different Land Cover Types and Seasons[a]

Land cover types	Statistic	Δ_{max}, °C		Δ_{min}, °C	
		May–Sept.	Oct.–Apr.	May–Sept.	Oct.–Apr.
Crops and grasslands	Mean	−1.45	−1.81	−3.08	−3.96
	σ	1.71	1.60	1.08	1.11
	Sample size	77.00	83.00	44.00	80.00
Forests	Mean	−0.21	−0.77	−3.69	−4.45
	σ	1.34	1.43	1.23	1.12
	Sample size	40.00	45.00	24.00	41.00
	t-value	−4.158	−3.696	2.072	2.298

[a]σ values indicate standard deviation of Δ.
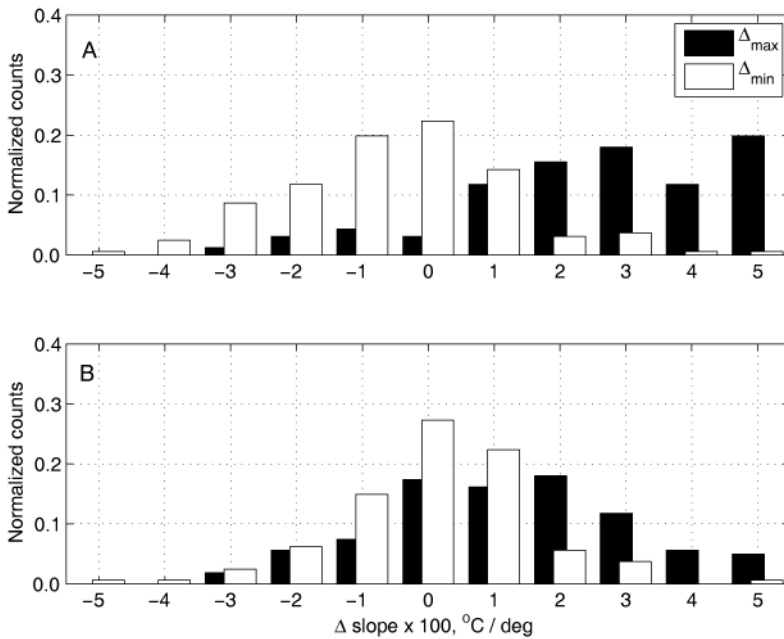
Fig. 9. Histograms of the slope parameter for linear regression between $\Delta = T_a - T_s$ and view zenith angle (Figs. 6 and 7). Counts in each bin were normalized by the total number of observations that are presented in Table 4 for May–Sept. (A) and Oct.–Apr. (B) periods.

Unlike the Δ_{max} case, the slope parameter of the regression between Δ_{min} and view angle is almost normally distributed with a small, noticeable shift toward negative values. This pattern is also consistent with predictions of weak θ dependence of T_s during nighttime hours. At the same time, there are no such peculiarities in the slope distribution between Δ_{max} and Δ_{min} during October–April (Fig. 9).
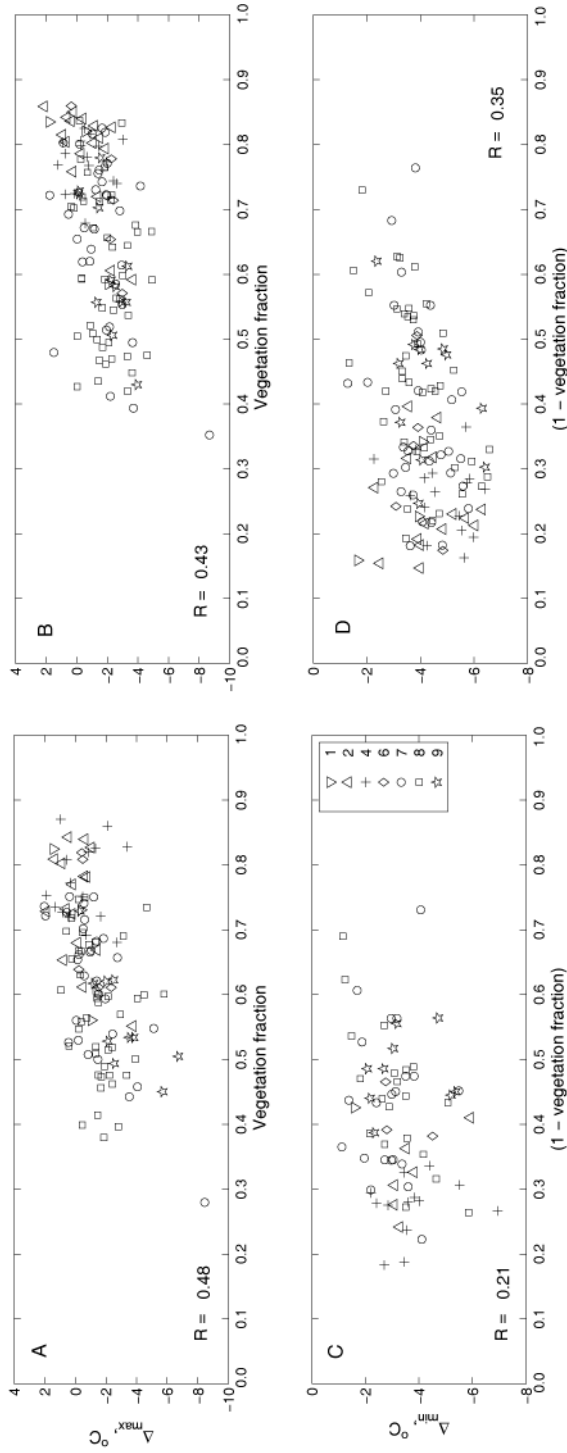
Fig. 10. Scatterplots between intercept parameter of linear regression between $\Delta = T_a - T_s$ and view zenith angle (Figs. 6 and 7) and vegetation fraction (f) or with $(1 - f)$ represented by averaged values within 0–40° interval of the MODIS zenith angle for May–Sept. (A, C) and Oct.–Apr. (B, D) 2000–2004 periods. R denotes correlation coefficient. The legend for the symbols indicating the land cover types is the same as in Figure 8.
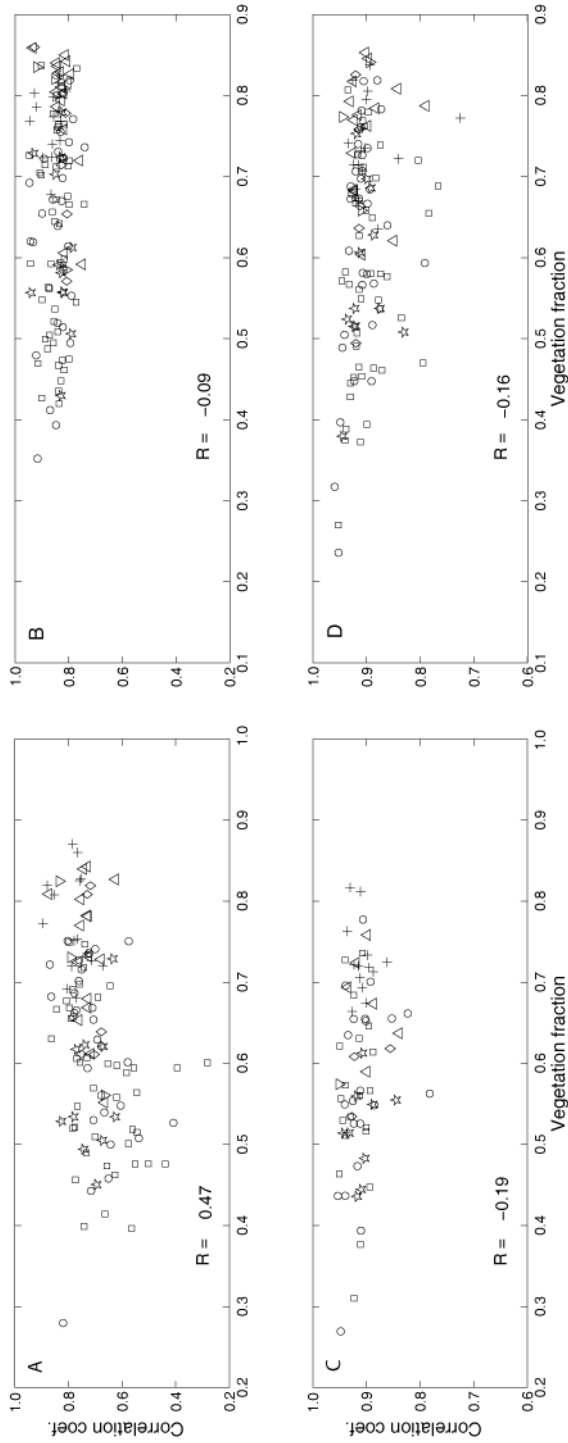
Fig. 11. Scatterplots between vegetation fraction and correlation coefficient between T_a^{max} and LST (A, B) and between T_a^{min} and LST (C, D). May–Sept. (A, C) and Oct.–Apr. (B, D) periods. Legend for the symbols indicating the land cover types is the same as in Figure 8.

Taking into account the relatively small values of the slope, within ± 0.01°C/deg range (Fig. 9), the regression intercept parameter can be considered as a mean estimate of the Δ value. Figure 8 illustrates the geographical distribution of mean Δ_{max} values for the May–September and October–April periods generated by cubic spline interpolation from station points. Additionally, Figure 8 shows symbols at station locations indicating a dominant MODIS PFT category within 1.0 km^2 using a land cover classification derived from MOD12Q1. Applying other classifications like the International Geosphere-Biosphere Programme Scheme did not significantly alter the results (Townshend et al., 1994).

Considering fields of Δ_{max} and cover types together allows us to conclude that the temperature difference Δ_{max} is negative, in general, over crops and grassland pixels (PFT types 6-8) and usually is slightly positive over forests (PFT types 1-4). Table 4 provides solid support for this preliminary inference. The mean value of Δ_{max} changes from –1.45°C (–1.81°C) for the crops and grasslands to –0.2°C (–0.77°C) for the forest cover types during the May–September period.[5] The observed changes in the mean values of Δ_{max} and Δ_{min} between various cover types shown in Table 4 are statistically significant at the 99% and 95% levels, respectively. These results are also in good qualitative agreement with Figure 8 in Goetz (1997), showing a systematic decrease in the surface temperature with an increase of the green vegetation fraction measured by the spectral vegetation index.

Figure 10 illustrates scatterplots between Δ_{max} and f and between Δ_{min} and (1-f) for all available stations over the study area. Both for the May–September and October–April periods, the relationship between Δ_{max} and f proves to be closer than between Δ_{min} and f, with R values of 0.48 and 0.43, respectively. Figure 11 shows scatterplots of the correlation coefficient between $T_a(max/min)$ and LST (10:30 AM/PM) versus the vegetation cover f. There was no apparent relationship between values of these correlations and cover types and vegetation fractions except for correlations between T_a^{max} and LST at 10:30 AM during the May–September period (Fig. 11A). The smallest scattering of R values with f is observed for T_a^{max} versus LST during October–April (Fig. 11B). R demonstrated rather broad variations between different stations, even for fixed cover types and the same range of f. These substantial variations of R could be associated with surface heterogeneity at the sub-pixel scale, and we intend to analyze this link in future work.

CONCLUSIONS

MODIS TIR LST measurements can be used for linear regression estimates of daily air maximum and minimum temperatures for any geographical region. If the correlation level between the air temperature and LST is high, assimilation of these estimates can improve the local/regional accuracy of air temperature fields produced by spatial interpolation from point surface observations. This property of the LST satellite product is of particular importance for various environmental and ecological models, which require the surface air temperature fields with a spatial resolution of about 1 km^2. Predictions of these models depend critically on the quality of input

---

[5]Numbers in parentheses correspond to values for the October–April season.

fields. Previous studies also showed the benefits of using nighttime LST as a valuable predictor for operational forecasts of the daily air minimum temperature.

The correlation coefficient (R) and the difference between the air temperatures and LSTs have shown rather consistent variations with pixel resolution, view zenith angle of the MODIS instrument, satellite overpass time, season, land-cover type, and the vegetation fraction over the state of Mississippi during the years 2000–2004. While R values between maximum temperature and LST were well stratified and separated depending on season (May–September or October–April) and time of day (maximum or minimum temperature), there were no certain indications for any dependence of R on cover type and the vegetation fraction. Therefore, seasonal weather variability (related to the frequency and intensity of cold atmospheric fronts affecting the study area) has proven to be more important than surface cover as a factor controlling observed level of R at 1.0 and 5.0 km^2 aggregation scales of MODIS LST data.

The difference between maximum air temperature and LST demonstrated linear increase with view angle (1–2°C for angle changes from 0° to ±65°) and remained constant or slightly decreased in case of the daily air minimum temperature. These changes were in a good agreement with predictions from a simple mixed-pixel model including both bare soil and vegetation-cover components of the TIR signal. While an average interpolation accuracy of 1–2°C for air temperature is acceptable by some applications, angle dependence can be neglected. By using LST data selected by applying the view zenith angle threshold (±40° or ±20°), interpolation accuracy can be improved at some locations while effectively reducing the availability of LST data, and therefore indirectly lowering the quality of representation (spatial detail) of the interpolated air temperature.

On average during May–September, the absolute value of this difference revealed a marked reduction by 1°C over more vegetated areas such as forests in comparison with less vegetated or more open ground such as crops or grassland. This feature was more distinct for the difference between maximum air temperature and LST, and was in overall qualitative agreement with numerous previous findings. This demonstrated that LST decreased linearly and approached screen air temperature asymptomatically as long as the fraction of the green vegetation cover increased.

The contribution of non-linear effects associated with non-zero spatial covariations between variables involved in the surface energy balance equation has been proven to be negligible for temperature terms; the covariation contribution to the mean difference between air temperature and LST was <1% for a typical range of environmental variables. Sampling data from all-day clear skies based on hourly *in situ* observations resulted in a statistically significant improvement of correlation and in a lowering of the standard deviation for difference between air temperature and 5.0 km^2 LST. This result indicates a marked degradation of the relationship between air temperature and LST due to partly-cloudy sky and sub-pixel cloudiness.

Both Terra and Aqua high-resolution LST exhibited a small, but persistent, increase in correlation between the air temperature and LST, as compared with the coarse-resolution LST. However, the overall improvement was not as much as might be expected from using higher resolution. Changing from Terra to Aqua LST did not substantially alter estimated correlations, indicating that a time difference between the moment of the satellite overpass and the time when maximum or minimum air

temperature was observed was not critical for controlling the correlation level between air temperature and LST. This inference was also supported by exceptionally strong correlations ($R \geq 0.99$) observed between maximum air temperature and that of measured at 10:30 AM. These high R values for air temperatures suggested that factors other than the time difference acting to lower observed correlations and to increase scattering between the air temperature and LST. Therefore, Terra globally gridded LST fields (MODIS name MOD11C1) with coarse resolution are probably most useful for regression estimates of the screen air temperatures, implying a certain tradeoff between better spatial coverage and quality/accuracy of this LST product in comparison with the high-resolution fields.

ACKNOWLEDGMENTS

REFERENCES

Bolstad, P. V., Swift, L., Collins, F., and J. Régnière, 1998, "Measured and Predicted Air Temperatures at Basin to Regional Scales in the Southern Appalachian Mountains," *Agricultural and Forest Meteorology*, 91:161-176.

Brutsaert, W., 1982, *Evaporation into the Atmosphere, Theory, History, and Applications*, Boston, MA: D. Reidel, 219 p.

Campbell, G. S. and J. M. Norman, 1998, *An Introduction to Environmental Biophysics,* 2nd ed., New York, NY: Springer-Verlag, 286 p.

Caparrini, F., Castelli, F., and D. Entekhabi, 2003, "Mapping of Land-Atmosphere Heat Fluxes and Surface Parameters with Remote Sensing Data," *Boundary-Layer Meteorology*, 107:605-633.

Carlson, T. N. and D. A. Ripley, 1997, "On the Relation between NDVI, Fractional Vegetation Cover, and Leaf Area Index," *Remote Sensing of Environment*, 62:241-252.

Cressie, N. A., 1991, *Statistics for Spatial Data*, New York, NY: John Wiley & Sons, 900 p.

Doraiswamy, P. C., Hatfield, J. L., Jackson, B., Akhmedov, B., Prueger, J., and A. Stern, 2004, "Crop Condition and Yield Simulations using Landsat and MODIS," *Remote Sensing of Environment*, 92:548-559.

Florio, E. N., Lele, S. R., Chi Chang, Y., Sterner, R., and G. E. Glass, 2004, "Integrating AVHRR Satellite Data and NOAA Ground Observations to Predict Surface Air Temperature: A Statistical Approach," *International Journal of Remote Sensing*, 25:2979-2994.

Focks, D. A., Daniels, E., Heile, D. G., and J. E. Keesling, 1995, "A Simulation-Model of the Epidemiology of Urban Dengue Fever: Literature Analysis, Model

Development, Preliminary Validation, and Samples of Simulation Results," *American Journal of Tropical Medicine And Hygiene*, 53:489-506.

Friedl, M. A., 1995, "Modeling Land Surface Fluxes Using a Sparse Canopy Model and Radiometric Surface Measurements," *Journal of Geophysical Research*, 100:25,435-25,446.

Friedl, M. A., 2002, "Forward and Inverse Modeling of Land Surface Energy Balance Using Surface Temperature Measurements," *Remote Sensing of Environment*, 79: 344-354.

Gallo, K. P. and C. S. T. Daughtry, 1987, "Differences in Vegetation Indices for Simulated Landsat-5 MSS and TM, NOAA-9 AVHRR, and SPOT-1 Sensor Systems," *Remote Sensing of Environment*, 23:439-452.

Gallo, K. P., McNab, A. L., Karl, T. R., Brown, J. F., Hood, J. J., and J. D. Tarpley, 1993, "The Use of NOAA AVHRR Data for Assessment of the Urban Heat Island Effect," *Journal of Applied Meteorology*, 32:899-908.

Gao, W., 1995, "Parameterization of Subgrid-Scale Land Surface Fluxes with Emphasis on Distributing Mean Atmospheric Forcing and Using Satellite-Derived Vegetation Index," *Journal of Geophysical Research*, 100:14,305-14,317.

Garratt, J. R., 1992, *The Atmospheric Boundary Layer*, New York, NY: Cambridge University Press, 316 p.

Gash, J. H. C., 1987, "An Analytical Framework for Extrapolating Evaporation Measurements by Remote Sensing Surface Temperature," *International Journal of Remote Sensing,* 8:1245-1249.

Goetz, S. J., 1997, "Multi-sensor Analysis of NDVI, Surface Temperature and Biophysical Variables at a Mixed Grassland Site," *International Journal of Remote Sensing*, 18:71-94.

Gutman, G. and A. Ignatov, 1998, "The Derivation of the Green Vegetation Fraction from NOAA/AVHRR Data for Use in Numerical Weather Prediction Models," *International Journal of Remote Sensing*, 19:1533-1543.

Holland, P. W. and R. E. Welsch, 1977, "Robust Regression Using Iteratively Reweighted Least-Squares," *Communications in Statistics: Theory and Methods*, A6: 813-827.

Hope, A., Engstrom, R., and D. Stow, 2005, "Relationship between AVHRR Surface Temperature and NDVI in Arctic Tundra Ecosystems," *International Journal of Remote Sensing*, 26:1771-1776.

Houborg, R. M. and H. Soegaard, 2004, "Regional Simulation of Ecosystem CO_2 and Water Exchange for Agricultural Land Using NOAA AVHRR and Terra MODIS Satellite Data. Application to Zealand, Denmark," *Remote Sensing of Environment*, 93:150-167.

Jin, M. and R. E. Dickinson, 2002, "New Observational Evidence for Global Warming from Satellite," *Geophysical Research Letters,* 29:10.1029/2001GL013833.

Jin, M., Dickinson, R. E., and A. M. Vogelmann, 1997, "A Comparison of CCM2-BATS Skin Temperature and Surface Air Temperature with Satellite and Surface Observations," *Journal of Climate*, 10:1505-1524.

Jones, P., Jedlovec, G., Suggs, R., and S. Haines, 2004, "Using MODIS LST to Estimate Minimum Air Temperatures at Night," in *13th Conference on Satellite Meteorology and Oceanography* (preprints), Norfolk, VA: AMS, 4.13 (CD-ROM).

Kawashima, S., Ishida, T., Minomura, M., and T. Miwa, 2000, "Relations between Surface Temperature and Air Temperature on a Local Scale during Winter Nights," *Journal of Applied Meteorology*, 39:1570-1579.

Knyazikhin, Y., Martonchik, J. V., Myneni, R. B., Diner, D. J., and S. W. Running, 1998, "Synergistic Algorithm for Estimating Vegetation Canopy Leaf Area Index and Fraction of Absorbed Photosynthetically Active Radiation from MODIS and MIRS Data," *Journal of Geophysical Research*, 103:32,257-32,275.

Kustas, W. P., Prueger, J. H., Humes, K. S., and P. J. Starks, 1999, "Estimation of Surface Heat Fluxes at Field Scale Using Surface Layer versus Mixed-Layer Atmospheric Variables with Radiometric Temperature Observations," *Journal of Applied Meteorology*, 38:224-238.

Louis, J. F., 1979, "A Parametric Model of Vertical Eddy Fluxes in the Atmosphere," *Boundary-Layer Meteorology*, 17:187-202.

Mahrt, L., and D. Vickers, 2004, "Bulk Formulation of the Surface Heat Flux," *Boundary-Layer Meteorology*, 110:357-379.

Mesinger, F., DiMego, G., Kalnay, E., Shafran, P., Ebisuzaki, W., Jovic, D., Woolen, J., Mitchell, K., Rogers, E., Ek, M., Fan, Y., Grumbine, R., Higgins, W., Li, H., Lin, Y., Manikin, G., Parrish, D., and W. Shi, 2004, "North American Regional Reanalysis," in *Proceedings of the 20th InternationalConference on Interactive Information and Processing Systems (IIPS) for Meteorology, Oceanography, and Hydrology*, Seattle, WA: 84th AMS Annual Meeting, 13 p. (CD-ROM).

MODIS Data Products, 2001, Land Processes Distributed Active Archive Center [http://edcdaac.usgs.gov/modis/dataproducts.asp].

Mostovoy, G. V., King, R., Reddy, K. R., and Kakani, V. G., 2005, "Using MODIS LST Data for High-Resolution Estimates of Daily Air Temperature Over Mississippi," in *Proceedings of the 3rd International Workshop on the Analysis of Multi-Temporal Remote Sensing Images*, May 2005, Biloxi, MS, IEEE 5 p. (CD-ROM).

Myneni, R. B., Hoffman, S., Knyazikhin, Y., Privette, J. L., Glassy, J., Tian, Y., Wang, Y., Song, X., Zhang, Y., Smith, G. R., Lotsch, A., Friedl, M., Morisette, J. T., Voltava, P., Nemani, R. R., and S. W. Running, 2002, "Global Products of Vegetation Leaf Area and Fraction Absorbed PAR from Year One of MODIS Data," *Remote Sensing of Environment*, 83:214-231.

NOAA NCDC (National Oceanic and Atmospheric Administration, National Climate Data Center), 2004, Climate Data Online [http://cdo.ncdc.noaa.gov/CDO /cdo].

Norman, J. M. and F. Becker, 1995, "Terminology in Thermal Infrared Remote Sensing of Natural Surfaces," *Agricultural and Forest Meteorology*, 77: 153-166.

Norman, J. M., Kustas, W. P., and K. S. Humes, 1995, "A Two-Source Approach for Estimating Soil and Vegetation Energy Fluxes from Observations of Directional Radiometric Surface Temperature," *Agricultural and Forest Meteorology*, 77: 263-293.

Oke, T. R., 1987, *Boundary Layer Climates*, 2nd ed., New York, NY: Methuen, 435 p.

Park, S., Feddema, J .J., and S. L. Egbert, 2005, "MODIS Land Surface Temperature Composite Data and Their Relationships with Climatic Water Budget Factors in the Central Great Plains," *International Journal of Remote Sensing*, 26:1127-1144.

Price, J. C., 1990, "Using Spatial Context in Satellite Data to Infer Regional-Scale Evapotranspiration," *IEEE Transactions on Geoscience and Remote Sensing,* 28:940-948.

Prihodko, L. and S. N. Goward, 1997, "Estimation of Air Temperature from Remotely Sensed Observations," *Remote Sensing of Environment*, 60:335-346.

Prince, D. T., McKenney, D. W., Nalder, I. A., Hutchinson, M. F., and J. L. Kesteven, 2000, "A Comparison of Two Statistical Methods for Spatial Interpolation of Canadian Monthly Mean Climate Data," *Agricultural and Forest Meteorology*, 101:81-94.

Prince, S. D., Goetz, S. J., Dubayah, R. O., Czajkowski, K. P., and M. Thawley, 1998, "Inference of Surface and Air Temperature, Atmospheric Precipitable Water and Vapor Pressure Deficit Using Advanced Very High-Resolution Radiometer Satellite Observations: Comparison with Field Observations," *Journal of Hydrology,* 212-213:230-249.

Reddy, K. R., Hodges, H. F., and J. M. McKinion, 1997, "Crop Modeling and Applications: A Cotton example," *Advances in Agronomy*, 59:225-290.

Reddy, K. R., Kakani, V. G., McKinion, J. M., and D. N. Baker, 2002, "Applications of a Cotton Simulation Model, GOSSYM, for Crop Management, Economic and Policy decisions," in *Agricultural System Models in Field Research and Technology Transfer*, Ahuja, L. R., Liwang Ma, and T. A. Howell (Eds.), Boca Raton, FL,: CRC Press, 33-73.

Régnière, J., 1996, "A Generalized Approach to Landscape-Wide Seasonal Forecasting in Temperature-Driven Simulation Models," *Enviromental Entomology*, 25:869-881.

Sandholt, I., Rasmussen, K., and J. Andersen, 2002, "A Simple Interpretation of the Surface Temperature/Vegetation Index Space for Assessment of Surface Moisture Status," *Remote Sensing of Environment*, 79:213-224.

Sun, J., Massman, W., and D. A. Grantz, 1999, "Aerodynamic Variables in the Bulk Formulation of Turbulent Fluxes," *Boundary-Layer Meteorology*, 91:109-125.

Sun, J. and L. Mahrt, 1995, "Determination of Surface Fluxes from the Surface Radiative Temperature," *Journal of the Atmospheric Sciences*, 52:1096-1106.

Tian, Y., Wang, Y., Zhang, Y., Knyazikhin, Y., Bogaert, J., and R. B. Myneni, 2002, "Radiative Transfer Based Scaling of LAI Retrievals from Reflectance Data of Different Resolutions," *Remote Sensing of Environment*, 84:143-159.

Townshend, J. R. G., Justice, C. O., Skole, D., Malingreau, J.-P., Cihlar, J., Teillet, P., Sadowski, F., and S. Ruttenberg, 1994, "The 1 km Resolution Global Dataset: Needs of the International Geosphere and Biosphere Programme," *International Journal of Remote Sensing*, 15:3417-3442.

Voogt, J. A. and C. S. B. Grimmond, 2000, "Modeling Surface Sensible Heat Flux Using Surface Radiative Temperatures in a Simple Urban Area," *Journal of Applied Meteorology*, 39:1679-1699.

Wan, Z., 1999, "MODIS Land-Surface Temperature Algorithm Theoretical Basis Document (LST ATBD)," Version 3.3, University of California, Santa Barbara, CA [http://www.icess.ucsb.edu/modis/LstUsrGuide/atbd_mod11.pdf].

Wan, Z. and J. Dozier, 1996, "A Generalized Split-Window Algorithm for Retrieving Land-Surface Temperature from Space," *IEEE Transactions on Geoscience and Remote Sensing*, 34:892-905.

Wan, Z. and Z.-L. Li, 1997, "A Physics-Based Algorithm for Retrieving Land-Surface Emissivity and Temperature from EOS/MODIS Data," *IEEE Transactions on Geoscience and Remote Sensing*, 35:980-996.

Wan, Z., Zhang, Y., Zhang, Q. and Z.-L. Li, 2002, "Validation of the Land-Surface Temperature Products Retrieved from Terra Moderate Resolution Imaging Spectroradiometer Data," *Remote Sensing of Environment*, 83:163-180.

Wan, Z., Zhang, Y., Zhang, Q., and Z.-L. Li, 2004, "Quality Assessment and Validation of the MODIS Global Land Surface Temperature," *International Journal of Remote Sensing,* 25:261-274.

Wittich, K-P. and O. Hansing, 1995, "Area-Averaged Vegetative Cover Fraction Estimated from Satellite Data," *International Journal of Biometeorology*, 38:209-215.

Zeng, X., Dickinson, R. E., Walker, A., Shaikh, M., DeFries, R. S., and J. Qi, 2000, "Derivation and Evaluation of Global 1-km Fractional Vegetation Cover Data for Land Modeling," *Journal of Applied Meteorology*, 39:826-839.